JGR Atmospheres

RESEARCH ARTICLE
10.1029/2022JD037513

Special Section:
Southern Ocean clouds, aerosols, precipitation and radiation

Important Ice Processes Are Missed by the Community Earth System Model in Southern Ocean Mixed-Phase Clouds: Bridging SOCRATES Observations to Model Developments

Xi Zhao[1], Xiaohong Liu[1], Susannah Burrows[2], Paul J. DeMott[3], Minghui Diao[4], Greg M. McFarquhar[5,6], Sachin Patade[7], Vaughan Phillips[7], Greg C. Roberts[8], Kevin J. Sanchez[9], Yang Shi[1], and Meng Zhang[10]

[1]Department of Atmospheric Sciences, Texas A&M University, College Station, TX, USA, [2]Atmospheric Sciences and Global Change Division, Pacific Northwest National Laboratory, Richland, WA, USA, [3]Department of Atmospheric Science, Colorado State University, Fort Collins, CO, USA, [4]Department of Meteorology and Climate Science, San Jose State University, San Jose, CA, USA, [5]Cooperative Institute for Severe and High Impact Weather Research and Operations, University of Oklahoma, Norman, OK, USA, [6]School of Meteorology, University of Oklahoma, Norman, OK, USA, [7]Department of Physical Geography and Ecosystem Science, Lund University, Lund, Sweden, [8]Scripps Institution of Oceanography, University of California, San Diego, CA, USA, [9]Universities Space Research Association, Columbia, MD, USA, [10]Lawrence Livermore National Laboratory, Livermore, CA, USA

Key Points:

- Important ice formation processes in Southern Ocean (SO) mixed-phase clouds are missed by the Community Earth System Model
- Sea spray organic aerosols contribute a larger fraction of ice nucleating particles over the SO than dust aerosols
- Secondary ice production processes are crucial for controlling ice crystal concentrations in moderately cold SO clouds

Supporting Information:

Supporting Information may be found in the online version of this article.

Correspondence to:

X. Liu,
xiaohong.liu@tamu.edu

Citation:

Zhao, X., Liu, X., Burrows, S., DeMott, P. J., Diao, M., McFarquhar, G. M., et al. (2023). Important ice processes are missed by the Community Earth System Model in Southern Ocean mixed-phase clouds: Bridging SOCRATES observations to model developments. *Journal of Geophysical Research: Atmospheres*, *128*, e2022JD037513. https://doi.org/10.1029/2022JD037513

Received 16 JUL 2022
Accepted 30 JAN 2023

Abstract Global climate models (GCMs) are challenged by difficulties in simulating cloud phase and cloud radiative effect over the Southern Ocean (SO). Some of the new-generation GCMs predict too much liquid and too little ice in mixed-phase clouds. This misrepresentation of cloud phase in GCMs results in weaker negative cloud feedback over the SO and a higher climate sensitivity. Based on a model comparison with observational data obtained during the Southern Ocean Cloud Radiation and Aerosol Transport Experimental Study, this study addresses a key uncertainty in the Community Earth System Model version 2 (CESM2) related to cloud phase, namely ice formation in pristine remote SO clouds. It is found that sea spray organic aerosols (SSOAs) are the most important type of ice nucleating particles (INPs) over the SO with concentrations 1 order of magnitude higher than those of dust INPs based on measurements and CESM2 simulations. Secondary ice production (SIP) which includes riming splintering, rain droplet shattering, and ice-ice collisional fragmentation as implemented in CESM2 is the dominant ice production process in moderately cold clouds with cloud temperatures greater than −20°C. SIP enhances the in-cloud ice number concentrations (Ni) by 1–3 orders of magnitude and predicts more mixed-phase (with percentage occurrence increased from 15% to 21%), in better agreement with the observations. This study highlights the importance of accurately representing the cloud phase over the pristine remote SO by considering the ice nucleation of SSOA and SIP processes, which are currently missing in most GCM cloud microphysics parameterizations.

Plain Language Summary For decades, global climate models (GCMs) have exhibited large biases in simulating the radiative budget over the Southern Ocean (SO), mainly due to the poor simulation of SO clouds. Understanding the ice formation processes in SO clouds is critically important to simulating cloud effects on radiation as well as cloud feedback to global warming. In this study, we conduct an integrated model-observational study to address a key area of uncertainty in GCMs, namely ice formation and evolution over the pristine SO. Model simulations of cloud and aerosol properties are compared against the observational data obtained during the Southern Ocean Cloud Radiation and Aerosol Transport Experimental Study. This study highlights the importance of accurately representing the cloud phase over the pristine remote SO by considering the ice nucleation of sea spray organic aerosols and secondary ice processes, which are currently missing in most GCM cloud microphysics parameterizations.

1. Introduction

Clouds cover 80%–90% of the SO region from an annual average perspective as indicated by satellite retrievals (Kay et al., 2012; Mace et al., 2009; Matus & L'Ecuyer, 2017; McCoy et al., 2014), making the SO one of the cloudiest regions on the Earth. Clouds over the SO are often mixed-phase in nature, and the cloud lifetime, phase partitioning, and precipitation efficiency are strongly impacted by the number of ice crystals in these clouds (Liu

et al., 2007; Mace et al., 2020; McFarquhar et al., 2021; Morrison et al., 2012; Vergara-Temprado et al., 2018; Wilson et al., 2015; Yang et al., 2021).

For decades, global climate models (GCMs) have exhibited large biases in simulating clouds and the radiative budget over the SO. The models participating in the Coupled Model Intercomparison Project Phase 5 (CMIP5) showed an excess in the surface shortwave radiation absorption over the SO (Bodas-Salcedo et al., 2016, 2019; Wang et al., 2018) partly due to their underpredicted cloud fraction and supercooled liquid water amount. On the contrary, some of the models participating in the latest CMIP Phase 6 (CMIP6) (e.g., Energy Exascale Earth System Model Version 1 (E3SMv1) and Community Earth System Model Version 2 (CESM2)) predicted too much supercooled liquid water over the SO (Zhang et al., 2019; Zhao, Liu, & Phillips, 2021). The misrepresentation of the cloud phase in GCMs further leads to incorrect cloud feedback over the SO through changes in cloud optical depth (Tan et al., 2019; Terai et al., 2016) and results in large uncertainties in modeled climate sensitivity (Gettelman et al., 2019; Murray et al., 2021; Tan et al., 2016, 2019; Zelinka et al., 2020).

The underestimation of cloud ice and overestimation of cloud liquid over the SO in CESM2 and E3SMv1 is a result of model misrepresentations of interactions among multiple cloud physical processes, especially between the ice nucleation schemes and the cloud microphysics schemes. The former schemes determine the production of ice crystals, while the latter schemes control the evolution of the ice populations. However, ice nucleation parameterizations in current GCMs are often derived based on measurements of dust aerosols and ice nucleating particles (INPs) over the Northern Hemisphere (NH) (DeMott et al., 2010, 2015; Meyers et al., 1992; Niemand et al., 2012). Dust aerosols have limited presence over the SO, with the averaged dust mixing ratio lower than 0.5 μg m^{-3} in the boundary layer, compared with that over the NH dust source and outflow regions which can be higher than 100 μg m^{-3} (Ke et al., 2022; M. Wu et al., 2020). This leads to a limited amount of dust INPs over SO. Since the ice nucleation in mixed-phase clouds is initiated by INPs and the SO is limited with dust INPs, how ice initiates and evolves over the SO is not well understood due to a lack of observations.

The importance of several processes has been identified to explain ice formation over the SO, benefiting from new observations over the SO, such as those obtained during Southern Ocean Cloud Radiation and Aerosol Transport Experimental Study (SOCRATES) and the Clouds Aerosols Precipitation Radiation and Atmospheric Composition over the Southern Ocean (CAPRICORN) campaigns. The leading ideas involve the contribution from immersion ice nucleation on sea spray organic INPs (DeMott et al., 2016; Vergara-Temprado et al., 2018; Wilson et al., 2015; Zhao, Liu, Burrows, et al., 2021) and secondary ice production (SIP) (Y. Huang et al., 2017; Mace et al., 2020; McFarquhar et al., 2021).

Previous studies highlighted the importance of sea spray organic aerosol (SSOA) for accurate simulation of the aerosols over the pristine remote oceanic regions, and further indicated that SSOA is an important source of INPs over the SO and elsewhere. For example, McCluskey, Hill, et al. (2018), McCluskey, Ovadnevaite, et al. (2018), and McCluskey et al. (2019) demonstrated that SSOAs are the dominant immersion freezing INPs for mixed-phase clouds at Mace Head Research Station over the North Atlantic and for boundary layer clouds over the SO; Vergara-Temprado et al. (2018) found that the cloud reflectivity over SO is highly sensitive to SSOA INPs; Wilson et al. (2015) suggested that SSOA INPs are important for high latitude mixed-phase clouds; and Zhao, Liu, Burrows, et al. (2021) showed that the concentrations of SSOA INPs are 1 order of magnitude higher than those of dust INPs in the marine boundary layer clouds of the Southern Hemisphere (SH) high latitudes.

SIP includes the riming splintering, rain droplet shattering, ice-ice collisional fragmentation, and sublimation fragmentation (Field et al., 2017). Recent measurements indicate that SIP may be a critical process for ice formation over the SO and can help to explain the discrepancies between observed ice crystal and INP number concentrations. For example, Mace et al. (2020) demonstrated that SIP is important for ice formation in supercooled marine boundary layer clouds over the SO based on the CloudSat and Cloud-Aerosol Lidar and Infrared Pathfinder Satellite Observation (CALIPSO) data. Y. Huang et al. (2017) suggested that SIP plays a dominant role in producing the high Ni measured in open cellular mixed-phase shallow convection over the SO whereas J. S. O'Shea et al. (2017) found that SIP increases the ice number concentrations by 1–3 orders of magnitude based on the measurements collected during the Microphysics of Antarctic Clouds (MAC) campaign in 2015. Using measurements from SOCRATES in combination with high-resolution numerical modeling, Lasher-Trapp et al. (2021) re-examined SIP in the Southern Ocean cumuli, and found that the measured Ni exhibits 7 orders of magnitude or more higher than INP number concentrations, which is also reproduced by their numerical modeling. Based on the global cloud-resolving simulations, Atlas et al. (2022) showed that including the riming

splintering process increases Ni in cumulus clouds and the shortwave cloud radiative effect becomes less negative (changed by 10 W m^{-2}) over the SO. Järvinen et al. (2022) found that the measured Ni concentrations are 1–2 orders of magnitude higher than the measured INP concentrations when the temperature is smaller than −10°C, and are up to 5 orders of magnitude higher when the temperature is larger than −10°C during SOCRATES. Their results also suggested the importance of other SIP in addition to the HM process on the ice production in SO clouds. Combining the observations from SOCRATES, CAPRICORN, the Measurements of Aerosols, Radiation and Clouds over the Southern Ocean (MARCUS), and Macquarie Island Cloud Radiation Experiment (MICRE), McFarquhar et al. (2021) emphasized the important role of SIP in ice formation over the SO. However, to what quantitative extent SIP contributes to the ice formation in the mixed-phase clouds over the SO is still unclear.

To bridge the gap between the latest observational findings and current model biases, our previous studies have implemented the parameterizations of ice nucleation on SSOA (Zhao, Liu, Burrows, et al., 2021) and SIP processes (Zhao, Liu, & Phillips, 2021) into CESM2 to improve the model representation of ice production processes in the high latitudes (Zhao & Liu, 2021, 2022). In this work, we conduct an integrated model-observational study to address a key area of uncertainty in CESM2, namely ice formation and evolution over the pristine SO. The paper is organized as follows: Section 2 introduces the model and in situ measurements. Section 3 presents the results and interpretation of the results. Section 4 concludes the key findings of this study.

2. Model and Observation Data

2.1. Model Description

The model used in this study is the CESM2 (Danabasoglu et al., 2020), which includes an atmospheric component called the Community Atmosphere Model Version 6 (CAM6). CAM6 features a 4-mode version of the modal aerosol module (Liu et al., 2012, 2016) (hereafter MAM4) to represent various aerosol processes, in which the marine biogenic sulfate is produced from the dimethyl sulfide (DMS) oxidation in the default model. CAM6 uses a double-moment cloud microphysical scheme (Gettelman & Morrison, 2015) (MG2), in which the only SIP process represented is rime splintering (also known as Hallett-Mossop (HM) process, Hallett & Mossop, 1974). Cloud droplet nucleation is described by the Abdul-Razzak and Ghan (2000) scheme, which is based on Köhler's theory. Heterogeneous ice nucleation in mixed-phase clouds is represented by the classical nucleation theory (Hoose et al., 2010; Wang et al., 2014), which considers the immersion freezing, deposition nucleation, and contact freezing of dust and black carbon aerosols as INPs. Ice nucleation in cirrus clouds follows Liu and Penner (2005), which considers the competition between the homogeneous freezing of sulfate solution droplets and the heterogeneous freezing of dust aerosol. CAM6 uses the Cloud Layers Unified By Binormals (CLUBB) scheme (Golaz et al., 2002; Larson et al., 2002) for a unified treatment of cloud macrophysics, turbulence, and shallow convection. The deep convection process is treated by the Zhang and McFarlane (1995) scheme.

2.1.1. Emission, Activation, and Ice Nucleation of SSOA

The emission of primary SSOA is implemented in CAM6 by Zhao, Liu, Burrows, et al. (2021). The emission rate of sea spray aerosol (sea salt and SSOA) depends on 10-m wind speed and sea surface temperature. The OCEANFILMS approach (Organic Compounds from Ecosystems to Aerosols: Natural Films and Interfaces via Langmuir Molecular Surfactant) (Burrows et al., 2014, 2022) is used to parameterize organic fraction of the emitted sea spray aerosol. Different from earlier empirical chlorophyll-based schemes (e.g., Gantt et al., 2011), this physically based emission scheme adopts a Langmuir isotherm-based method to calculate the organic matter fraction of emitted sea spray aerosol. The emission scheme, which is described in detail in Burrows et al. (2014), lumps surface-active ocean macromolecules into three broad classes: lipid-like, protein-like, and polysaccharide-like. The effect of this scheme is to add SSOA mass as an internal mixture with the emitted sea salt, while also increasing the sea spray number emissions proportionally; this moderately increases the total Aitken and accumulation mode emissions in regions with ocean biological activity, with larger relative impacts at high latitudes (Burrows et al., 2022; Zhao, Liu, Burrows, et al., 2021).

Once in the atmosphere, the droplet nucleation of SSOA is treated by the Abdul-Razzak and Ghan (2000) scheme, with a density of 1,700 kg m^{-3} and hygroscopicity of 0.1 for SSOA (Zhao, Liu, Burrows, et al., 2021). The ice nucleation of SSOA is parameterized based on McCluskey, Ovadnevaite, et al. (2018) (M18), which was implemented in CAM6 by Zhao, Liu, Burrows, et al. (2021). M18 is a surface-active site density-based empirical scheme for deterministic immersion freezing on SSOA. M18 was developed based on the correlation between the

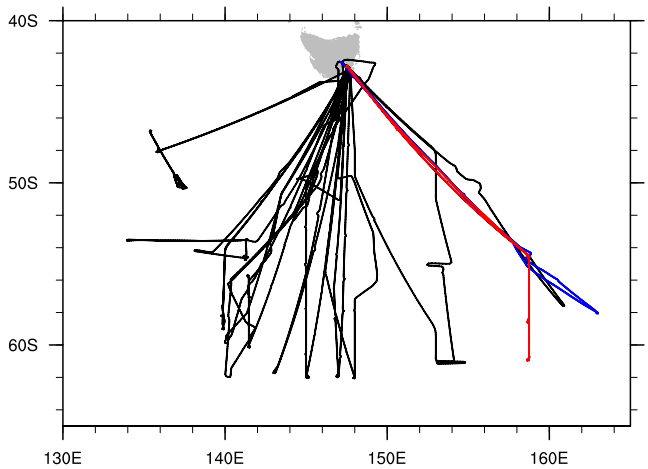

Figure 1. Flight tracks from SOCRATES NSF G-V aircraft. Blue is RF07 Flight on January 31, 2018, and red is RF09 Flight on February 4, 2018.

INP concentrations, outside of episodic periods of highly enhanced marine organics, and ambient aerosol surface area measured at the Mace Head Station in August 2015. The INP number concentration (N_{INP}) is calculated from the sea spray aerosol number concentration (N_{tot}), sea spray aerosol surface area (S_{ae}, calculated based on dry diameters of particles in Aitken and Accumulation modes) and the ice-active surface site density ($n_s(T)$) at a given temperature T, shown as

$$N_{INP}(T) = N_{tot} S_{ae} n_s(T) \quad (1)$$

in which $n_s(T)$ at a given temperature T is expressed as:

$$n_s(T) = e^{(-0.545(T-273.15)+1.0125)} \quad (2)$$

Note that the parameterization is based on a limited sample and may not be representative of the entire SO.

2.1.2. Secondary Ice Production

In addition to the riming splintering or HM mechanism in the default CAM6, Zhao, Liu, and Phillips (2021) implemented two other SIP mechanisms in CAM6: rain droplet shattering and ice-ice collisional fragmentation. The ice-ice collisional breakup is parameterized based on Phillips, Yano, and Khain (2017) and Phillips, Yano, Formenton, et al. (2017), which relates the number of ice fragments produced by SIP to ice particle kinetic energy and ice habits. The shattering during rain droplet freezing contains two modes (Phillips et al., 2018). In the first mode, the freezing of raindrops is triggered by collisions with INPs or small ice crystals, while in the second mode, the freezing of raindrops is caused by collisions between raindrops and more massive ice particles. To accurately represent the particle-scale (∼100 μm) SIP processes in GCMs with a horizontal resolution of ∼100 km, an emulated bin framework was developed for the bulk cloud microphysical scheme (Zhao, Liu, & Phillips, 2021).

2.1.3. Model Configuration and Experiments

All the model experiments are conducted in the nudged configuration (also known as specific dynamics), in which the temperature and winds are relaxed to the NASA Modern-Era Retrospective analysis for Research and Applications, Version 2 (MERRA2) (Molod et al., 2015) reanalysis data every 3 hr. The model horizontal resolution is 1.25 longitude by 0.9 latitude (∼100 km over the SO region), with 32 vertical levels up to 3 hPa. The model time step is 30 min. Model experiments were spun up for 1 year starting January 1, 2017 and ran continuously over the SOCRATES campaign period (from January 15 to February 26, 2018) for another 2 months. We archived the model outputs along the SOCRATES flight tracks with a 1-min frequency, with a method similar to C. Wu et al. (2017).

The control experiment (CTL) uses the default CAM6 model. The SSOA experiment is the same as CTL but uses CAM6 with added emission, activation, and ice nucleation of SSOA. The SIP experiment is the same as CTL but uses CAM6 with added SIP from droplet shattering and ice-ice collisional breakup processes.

2.2. Observation Data

The principal objective of the SOCRATES campaign was to improve the understanding of aerosol-cloud-radiation interactions with respect to the major synoptic-scale weather systems over the SO and to reduce the uncertainties related to clouds, aerosols, radiation, and their feedbacks in climate models (McFarquhar et al., 2021). SOCRATES used the National Science Foundation (NSF) Gulfstream-V (GV) research aircraft to collect measurements from January 15 to February 26, 2018, over the SO from 133°W to 163°W and 42°S to 62°S. The SOCRATES flights targeted the cold sector of cyclones where models show large bias (Figure 1). Fifteen flights were conducted to collect the observational data on aerosol, clouds, and precipitation.

The cloud condensation nuclei (CCN) data were measured with a miniature continuous-flow stream-wise thermal gradient chamber onboard the GV research aircraft (Roberts and Nenes, 2005), and CCN spectra were derived from the CCN scanning data with the supersaturation range from 0.10% to 0.85% and an interval of 0.05%. The

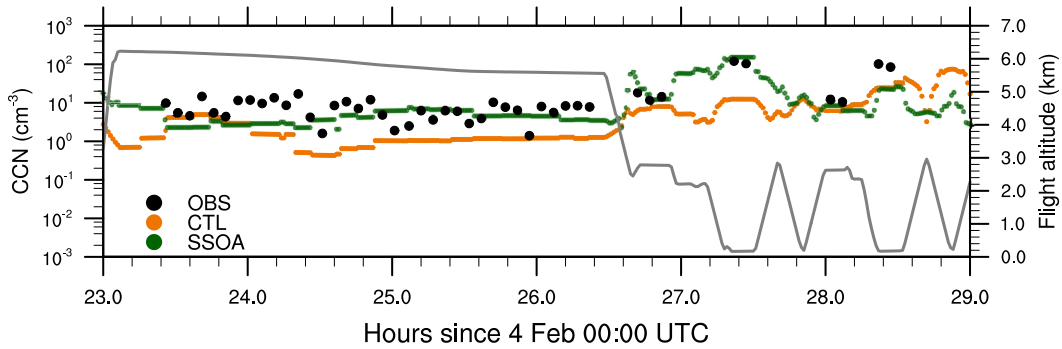

Figure 2. Time series of surface cloud condensation nuclei (CCN) concentrations at 0.1% supersaturation from measurements (black dots), control experiment (CTL) (orange line), and sea spray organic aerosol (SSOA) (green line) experiments along the flight track from RF09. The flight altitude is shown as the gray line.

INP data used in this study were measured by the Colorado State University (CSU) Continuous Flow Diffusion Chamber (CFDC) and the CSU ice spectrometer (IS) during the first CAPRICORN (McCluskey, Hill, et al., 2018) and SOCRATES campaigns (https://data.eol.ucar.edu/dataset/552.045). A suite of probes on the GV aircraft measured the cloud microphysical properties. As the processing of these data is detailed elsewhere (Wang et al., 2020; D'Alessandro et al., 2021; McFarquhar et al., 2021), only the most salient features are reviewed here. The phase of each 1-s period was determined using information from the Cloud Droplet Probe (CDP), Rosemount icing detector, and a multinomial logistic regression applied to images acquired by the 2-Dimensional Stereo (2DS) probe, with a subsequent manual adjustment through inspection of particles imaged by the 2DS Particle Habit Imaging and Polar Scattering probe PHIPS-HALO. Data from a King probe determined the bulk liquid water content (LWC), which had a correlation coefficient of 0.96 with LWC estimated from the CDP size distribution. Due to a small and highly uncertain depth of field for particles with maximum dimensions smaller than 200 μm ($D < 200$ μm) imaged by the 2DS (Baumgardner & Korolev, 1997; S. O'Shea et al., 2021), the ice crystal concentration used here only represents particles with $D > 200$ μm as derived by the University of Illinois/Oklahoma Optical Array Probe Processing Software (UIOOPS; McFarquhar et al., 2018). To be consistent with observations, the simulated Ni only considers ice particles with $D > 200$ μm. Although the Counterflow Virtual Impactor (CVI) and University of Colorado Closed-Path Hygrometer (CLH-2) measure total water content (TWC), estimations of IWC are not possible because the TWC is typically dominated by supercooled water. Thus, following Wang et al. (2020), the IWC was obtained using the 2DS number distribution functions, particle sizes, and projected area distributions following Baker and Lawson (2006). Because the observed IWC and ice water path (IWP) cannot distinguish cloud ice from snow, to be consistent with the observations, the simulated IWC and IWP both include snow component.

3. Results

3.1. Importance of Sea Spray Organic Aerosols to Southern Ocean Clouds

3.1.1. CCN Effect

Figure 2 compares the temporal evolution of simulated CCN from the CTL and SSOA experiments with CCN measured at 0.1% supersaturation along the tracks of research flight (RF) 09 (Figure S2 in Supporting Information S1 shows the comparison at 0.2% supersaturation). Overall, the CCN number concentrations in the CTL experiment are lower than 10 cm^{-3}, and underestimate the observations by up to 2 orders of magnitude for the 28-hr period following February 4 0:00 UTC. The mean value of CCN concentrations is 7.5 cm^{-3} in CTL averaged over RF09, which is significantly lower than the mean measured value of 26.7 cm^{-3}. This underestimation of CCN concentrations in the CTL experiment is very likely due to lacking the representation of SSOA in the default model, as previous studies (Burrows et al., 2014, 2022; W. T. K. Huang et al., 2018; Meskhidze et al., 2011; Zhao, Liu, Burrows, et al., 2021) highlighted the important contribution of SSOA to CCN in the remote marine atmosphere. Considering SSOA in the model doubles the simulated CCN concentrations to a mean value of 15.0 cm^{-3} in the SSOA experiment, which agrees better with the measurements. Moreover, the variation of CCN concentrations between 10^1 and 10^2 cm^{-3} (from 26.5 to 28.5 hr) in the measurements caused by the ramped

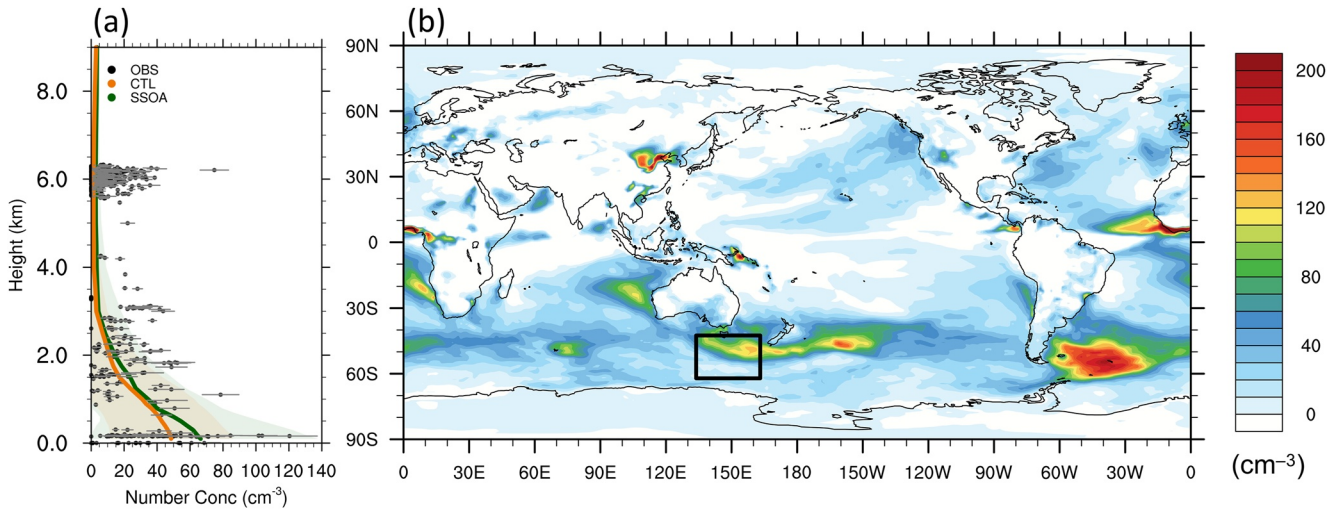

Figure 3. (a) Vertical distribution of cloud condensation nuclei (CCN) concentrations at 0.1% supersaturation from measurements (black solid dots), and the median values of CCN concentrations from the control experiment (CTL) (solid orange line) and sea spray organic aerosol (SSOA) (solid green line) experiments during all flights during the SOCRATES campaign. Colored shadings are 1-sigma standard deviations of model data, and horizontal gray lines represent 1-sigma standard deviations of measurements; (b) Spatial distribution of changes of surface CCN concentrations at 0.1% supersaturation due to SSOA (calculated by CCN_{-SSOA}-CCN_{-CTL}), using model data from January and February 2018. The black box indicates the SOCRATES campaign domain.

ascents and descents of the G-V indicates a strong reduction of CCN concentrations from the oceanic boundary layer to the free troposphere. This vertical variation is well captured by the SSOA experiment, but less so by the CTL experiment. As shown in Figure 2, the CCN concentrations are on the order of 10^2 cm^{-3} at 27.4 hr in the SSOA experiment and in the measurements, but only 10^1 cm^{-3} in the CTL experiment.

Figure 3a shows the vertical distribution of simulated and measured CCN concentrations at 0.1% supersaturation from all fights during SOCRATES. The median value of the surface CCN concentrations is increased from 50 cm^{-3} in CTL to 67 cm^{-3} in the SSOA experiment, and a notable increase in CCN concentrations is shown below 2 km (also shown in Sanchez et al. (2021)). This statistical analysis highlights the important contribution of SSOA to CCN concentrations in the boundary layer over the SO during the SOCRATES campaign.

The SSOA impact on the global spatial distribution of CCN concentrations is shown in Figure 3b as the change of surface CCN concentrations at 0.1% supersaturation. Figure 3b uses the simulation data from January and February 2018 to cover the SOCRATES campaign period. Boundary layer CCN concentrations over the SO are increased by 80 cm^{-3} on average as a result of considering SSOA in the model. The maximum increase (up to 100 cm^{-3} more) over the Indian Ocean is between 20°S and 30°S, while the maximum increase (up to 150 cm^{-3} more) over the Pacific Ocean is in the midlatitude region between 30°S and 50°S. The maximum increase (up to 300 cm^{-3} more) over the Atlantic Ocean is in the high latitudes between 45°S and 70°S. The regional increases in CCN concentrations are related to the ocean biological activity and high wind speeds over the storm tracks and the SO (Sanchez et al., 2021; Zhao, Liu, Burrows, et al., 2021).

SSOA strongly impacts CCN number concentrations in the SO boundary layer clouds and increases the CCN concentrations by an average of 50% and up to 2 orders of magnitude during the SOCRATES campaign. Considering SSOA in the model leads to better temporal evolution and vertical distributions of modeled CCN concentrations compared to the observations.

3.1.2. INP Effect

To evaluate the ability of SSOA to serve as INPs over remote high-latitude oceans, we compare model-simulated INP concentrations with the observations at different temperatures during the SOCRATES and CAPRICORN campaigns, as shown in Figure 4. Simulated SSOA INPs are calculated online using the M18 scheme (McCluskey, Ovadnevaite, et al., 2018), while dust INPs are calculated based on DeMott et al. (2015) (D15). A clear underestimation of observed INPs by 1–3 orders of magnitude at temperatures colder than −24°C is revealed particularly for the SOCRATES campaign if the model considers dust aerosol as the only source of INPs (Figure 4a). Our comparison with other sources of observed dust data (shown in Figure S3 in Supporting Information S1) suggests

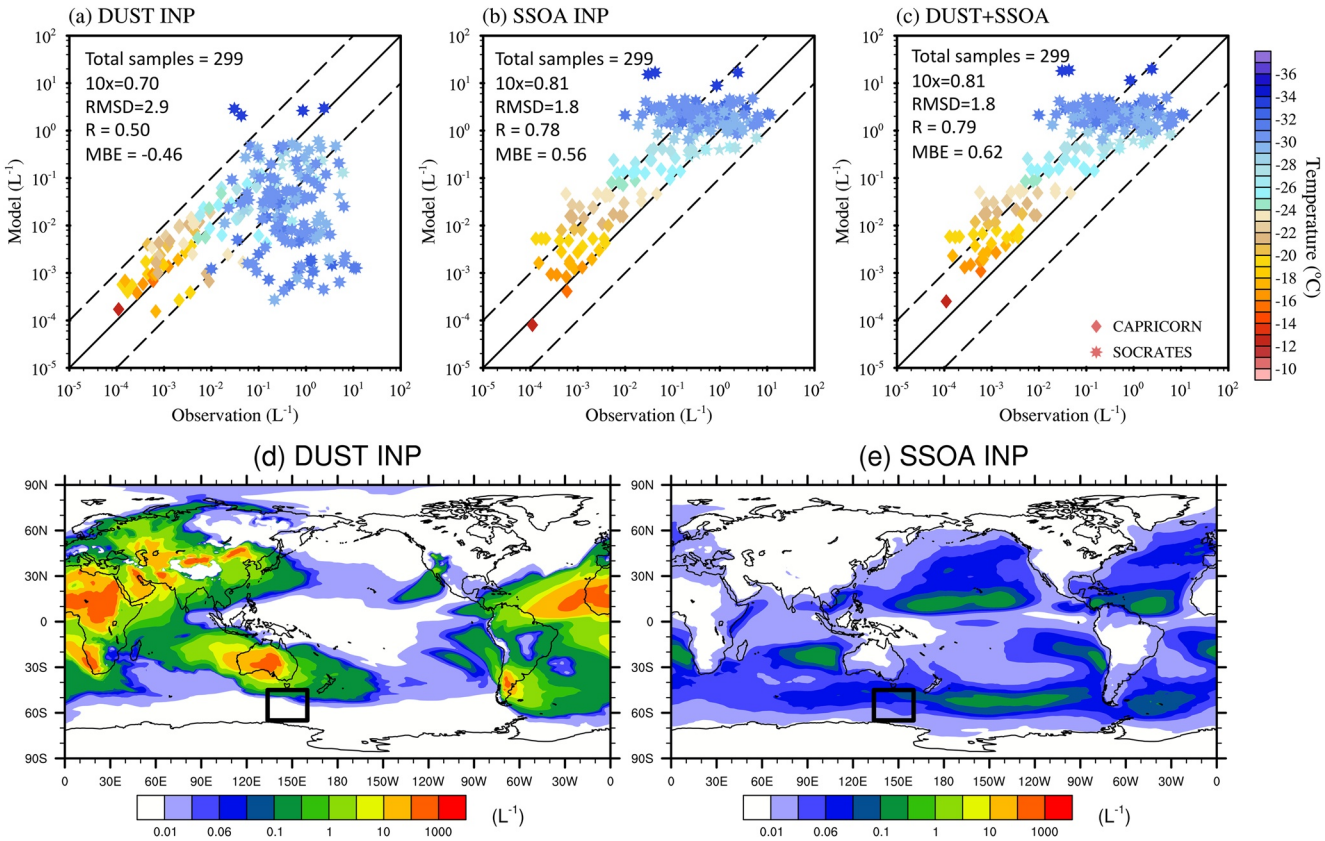

Figure 4. Comparison of simulated (a) DUST, (b) SSOA, and (c) DUST + SSOA INP versus measured INP number concentrations. Measured ice nucleating particles (INPs) were collected over the Southern Ocean during the CAPRICORN and SOCRATES campaigns. Simulated dust INPs are calculated online based on DeMott et al. (2015), and SSOA INPs are based on McCluskey, Ovadnevaite, et al. (2018). Error metrics for the comparison of modeled and observed INP concentrations include total number of samples, percentage of samples with simulated INPs within a factor of 10 of measurements (10×), root-mean-square-difference (RMSD), Spearman correlation (*R*), and mean bias error (MBE). Simulated INPs are sampled at the same altitudes, latitudes, and longitudes as the field measurements in (a), (b), and (c). Spatial distribution of 2-month averaged concentrations of (d) DUST INPs and (e) SSOA INPs, with INP concentrations diagnosed at a temperature of −25°C at 900 hPa. The black box indicates the SOCRATES campaign region.

that CESM2/CAM6 overestimates the observed dust concentrations over the SO (close to the SOCRATES region), likely because of too high dust emissions in the SH (Li et al., 2022; M. Wu et al., 2020). This indicates that the too low INPs when the model only considers dust aerosol is not due to the model underestimation of dust. A better agreement between measured and modeled INPs is obtained when both dust and SSOA are considered as sources of INPs. The Spearman correlation (*R*) increases from 0.5 (dust INPs only) to 0.79 (both dust and SSOA are considered), while the root-mean-square-difference (RMSD) decreases from 2.9 (dust INPs only) to 1.8 (both dust and SSOA are considered) as shown by the error metrics in Figures 4a and 4c. However, modeled INP number concentrations in the temperature range of −24°C to −28°C (Figure 4c) are nearly an order of magnitude higher than those of observed INPs. The possible factors for the bias could be that the model overestimates SSOA concentrations over the SO as shown in fig. 2a from Zhao, Liu, Burrows, et al. (2021) and/or the M18 scheme was developed based on the measurements at the Mace Head Station, which may not be representative of the cleaner environment over the SO. As shown in Figures 4a and 4b, SSOA INP concentrations are higher than those of dust INPs by 1–3 orders of magnitude. This is consistent with previous studies (McCluskey, Hill, et al., 2018, 2019; Vergara-Temprado et al., 2018; Wilson et al., 2015), which highlighted the dominant role of SSOA INPs as the seeds of ice crystals in mixed-phase clouds over pristine remote oceanic regions. From Figure 4d, dust INP concentrations are as high as 1000 L^{-1} over the land source regions, but are lower than 0.01 L^{-1} over the SO. In contrast, SSOA INP particles are prevalent over the oceans, with the maximum concentrations of 0.1 L^{-1} over the SO (Figure 4e). Note that Figures 4d and 4e are from a nudged simulation and averaged over the SOCRATES campaign period (i.e., austral summer). They are different from figs. 6a and 6b in Zhao, Liu, Burrows, et al. (2021) which shows the annually averaged dust and SSOA INPs based on a 20-year

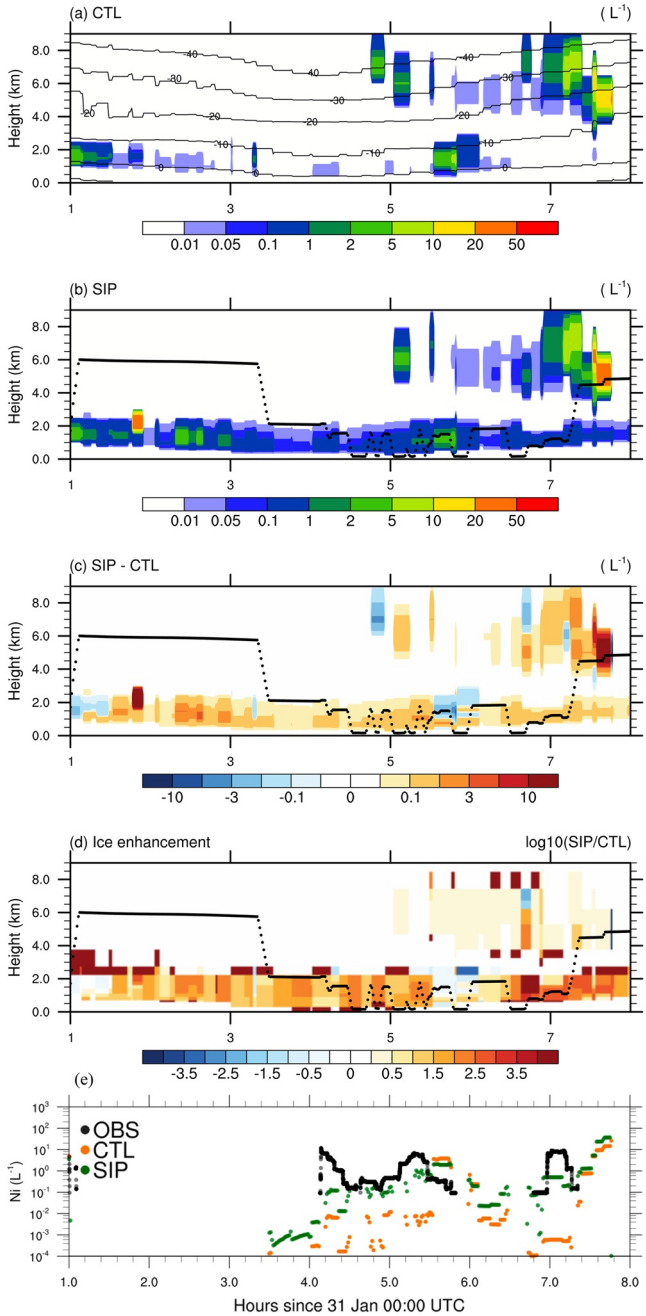

Figure 5. Time-height cross-section of ice number concentrations from (a) control experiment (CTL) experiment overlayed with temperature (solid black lines); (b) secondary ice production (SIP) experiment and (c) the difference of ice number concentrations between CTL and SIP experiments overlay with flight altitude (black dots); (d) ice enhancement ratio (IE, calculated as $IE = Ni_{\_SIP}/Ni_{\_CTL}$); and (e) time series of ice number concentrations for ice particles with diameter larger than 200 μm from CTL (orange dots), SIP (green dots), and measurement (black dots) along the flight track from RF07.

free-running simulation. Since the emissions of dust and SSOA vary strongly with the season, the dust and SSOA INPs can thus have different magnitudes and spatial distribution patterns between Figure 4 of this study and fig. 6 in Zhao, Liu, Burrows, et al. (2021).

In summary, SSOA is an important source of both CCN and INPs, which significantly influence the formation of clouds over the SO. We note that SSOA increases the CCN (at 0.1% supersaturation) by an average of 50% and up to 2 orders of magnitude locally in the near-surface air immediately above locations where the ocean biogeochemistry simulation outputs that are used to drive the OCEANFILMS scheme showed active phytoplankton blooms. Furthermore, the importance of SSOA to serve as INPs in the ice nucleation process is highlighted. The model underestimates the observed INP concentrations by 1–3 orders of magnitude if only dust INPs are considered. This underestimation is removed if both dust and marine INPs are considered in the model.

3.2. Importance of SIP to Southern Ocean Clouds

Figure 5 shows the SIP impact on the Ni and the associated ice enhancement ratio (IE), which is defined as $IE = Ni_{\_SIP}/Ni_{\_CTL}$. The top two panels show the time-height cross-section of Ni output from the CTL (Figure 5a) and SIP (Figure 5b) experiments along the RF07 flight track. Remarkable differences in Ni between the CTL and SIP experiments appear in the boundary layer clouds, where the CTL experiment predicts substantially lower concentrations (with an average value of 0.4 L^{-1}) compared to the SIP experiment (with an average value of 0.8 L^{-1}, as shown in Figure S1 in Supporting Information S1) consistent with the lack of a comprehensive representation of SIP processes in the default model used for the CTL experiment. Above 4 km, where the temperatures are below −20°C, Ni shows higher values relative to those in boundary-layer clouds, with averaged Ni of 0.6 and 1.3 L^{-1} from CTL and SIP (Figure S1 in Supporting Information S1), respectively. The maximum value of simulated Ni is around 10 L^{-1} above 4 km, which is much higher than ∼0.1 L^{-1} in boundary-layer clouds. The Ni difference between the boundary-layer and upper-level clouds is largely due to the ice nucleation, since the ice nucleation is more effective at lower temperatures.

The difference of Ni between SIP and CTL experiments is shown in Figure 5c and the IE ratio is shown in Figure 5d. A maximum absolute increase of Ni by 20 L^{-1} is noticed in the upper-level clouds at 4–6 km, and a relatively uniform but modest increase of Ni by 0.1–3 L^{-1} is shown in most of the boundary-layer clouds. In contrast, the IE ratio (i.e., the relative increase) shows maximum values for boundary-layer clouds with moderately low temperatures ($T > -20$°C), where the IE ratio can reach 4 orders of magnitude. For most of the colder clouds with temperatures less than −20°C above 5 km, the IE ratio is within 1 order of magnitude, although a maximum absolute increase of Ni is reported there.

The modeled Ni are compared to the aircraft measurements in Figure 5e along the RF07 flight track. Since the measurements only include ice particles with $D > 200$ μm, here we only include the modeled ice with a $D > 200$ μm. Overall, implementing SIP improves the agreement of model predicted Ni with the measurements. The CTL experiment shows a systematic underestimation of Ni by 1–4 orders of magnitude, except at 5.6–5.8 hr, when the CTL experiment overestimates Ni by 1 order of magnitude compared with the measurements. Generally, the Ni are increased by SIP by 1–3 orders of magnitude, and the Ni are around 10^{-1}, 10^{0}, and 10^{1} L^{-1} in CTL, SIP, and measurements, respectively, during the RF07. Furthermore, the overestimation of Ni in CTL at 5.6–5.8 hr is reduced after implementing SIP into the model.

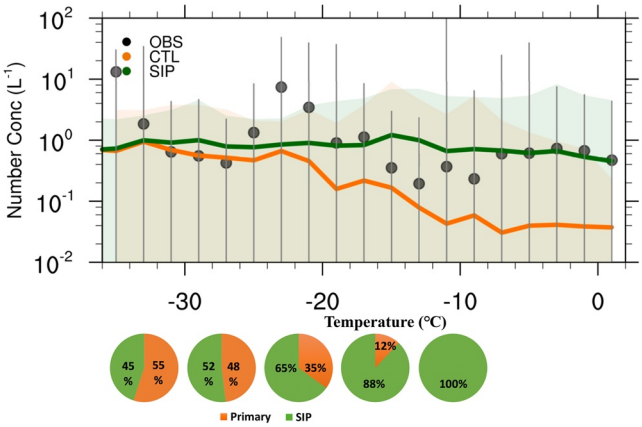

Figure 6. Median values of ice number concentrations from a suite of in situ probes (black dots), (b) control experiment (CTL) (orange line), and (c) secondary ice production (SIP) experiments (green line) as a function of temperature, binned at 2°C intervals for the entire SOCRATES campaign. The vertical gray lines represent standard deviations of measurements and colored shadings are standard deviations of model data. Pie charts show the relative contributions (calculated based on ice formation rates) from modeled primary ice nucleation and SIP processes averaged over 5°C temperature bins from −35°C to −10°C (i.e., −35°C to −30°C, −30°C to −25°C, −25°C to −20°C, −20°C to −15°C, and −15°C to −10°C from left to right).

In summary, a detailed comparison is conducted to investigate the SIP impact on Ni. We found that after the model considers SIP, a better agreement is achieved between the simulated and measured Ni, and the modeled Ni are enhanced by 1–3 orders of magnitude by the SIP processes.

Figure 6 shows the median values of simulated and measured Ni as a function of temperature for the entire SOCRATES campaign. CTL and SIP experiments give a similar performance and agree with the measured Ni reasonably well at temperatures less than about −25°C. However, at temperatures greater than −25°C, CTL underestimates Ni compared to observations, with the underestimation increasing with temperature. In particular, when the temperature is greater than −10°C, CTL underestimates the measured Ni by more than 1 order of magnitude. SIP simulation is more consistent with the observations. However, there is a discrepancy with observations for temperatures between −10°C and −18°C for both SIP and CTL. The SIP becomes important for $T > -20$°C, where Ni in the SIP experiment is 5–12 times that of the Ni in the CTL experiment. Relative contributions from primary ice nucleation and SIP from the SIP experiment are shown in the pie charts at different temperatures in Figure 6. It is clear that primary ice nucleation is more important than SIP at cloud temperatures less than −25°C, and the SIP is favored in moderately cold clouds with temperatures greater than −20°C, where Ni is enhanced by SIP by about 1 order of magnitude. The relative contributions of different SIP processes and primary ice nucleation at three temperature bins from −35°C to −10°C are further shown in Figure S4 in Supporting Information S1. As shown, ice-ice collisional breakup is the most important SIP process to ice formation for the SOCRATES clouds.

Figure 7 shows the probability of occurrence of liquid-phase, ice-phase, and mixed-phase clouds as a function of temperature. For the model data, mixed-phase cloud is defined as the liquid mass fraction between 0.1 and 0.9 (Yang et al., 2021). For the in situ measurement data, mixed-phase cloud is defined based on a phase identification algorithm (a combination of collocated airborne lidar, radar, and thermodynamic data) instead of liquid mass fraction (D'Alessandro et al., 2021; McFarquhar et al., 2021; Zaremba et al., 2020). Ice-only and liquid-only clouds are defined as the liquid mass fraction less than 0.1 and more than 0.9, respectively, for the measurement and model data. Ice-only and mixed-phase clouds are present in the measurements at temperatures greater than −5°C, and these ice particles are either seeding from the upper levels or newly formed through the SIP processes, considering that primary ice nucleation is limited at these temperatures. Moreover, a rapid increase in the frequency of occurrence of ice-only clouds once the temperature is lower than −20°C, and correspondingly, a rapid decrease in the frequency of occurrence of liquid-only clouds in the measurements, suggests the strong impact of the Wegener-Bergeron-Findeisen process on the cloud phase.

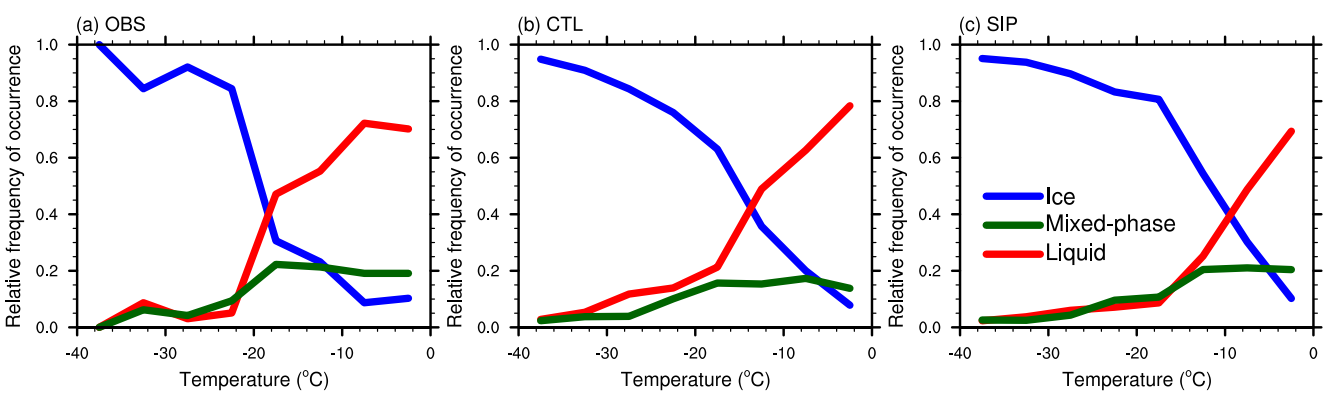

Figure 7. Relative occurrence frequency of liquid-phase, mixed-phase, and ice-phase clouds, denoted by red, green, and blue colors, respectively, derived from (a) a suite of in situ probes, (b) control experiment (CTL), and (c) secondary ice production (SIP) experiments as a function of temperature, binned at 5°C intervals for the 15 flights during the entire SOCRATES campaign.

Table 1
Relative Occurrence Frequency of Liquid-Phase, Mixed-Phase, and Ice-Phase Clouds for Cloud Temperatures Larger Than −20°C From 15 Flights During the SOCRATES Campaign, From the Measurements (OBS), CTL, and SIP Simulations

	OBS	CTL	SIP
Ice-phase clouds	0.14	0.22	0.31
Mixed-phase clouds	0.20	0.15	0.21
Liquid-phase clouds	0.66	0.63	0.48

Generally, the CTL experiment overestimates the frequency of occurrence of ice-only clouds and underestimates the occurrence of mixed-phase clouds during SOCRATES, especially when cloud temperature is greater than −20°C, as shown in Table 1. We note that the CTL experiment underestimates IWP (i.e., vertically integrated ice mass) on the global mean (Figure 8d). Overall, SIP results in more mixed-phase and ice-only clouds, and less liquid-only clouds over the SO, which leads to too much ice-only clouds and too few liquid-only clouds compared to the measurements. The occurrence frequency of mixed-phase clouds with temperatures larger than −20°C during the SOCRARES campaign is 20%, 15%, and 21% from measurements, CTL, and SIP, respectively (Table 1). This is consistent with our previous result in the Arctic regions, where SIP contributes to an increased occurrence of mixed-phase and ice clouds compared with the CTL simulation (Zhao, Liu, & Phillips, 2021).

3.3. Global Climate Implications

Figure 8 shows annual and zonal means of surface concentrations of CCN at 0.1% supersaturation, and cloud properties (IWC, LWP, and IWP) from model experiments in comparison with available satellite retrievals. The SSOA experiment shows the largest boundary layer CCN number concentration at 0.1% supersaturation with the global mean value of 107 cm^{-3}, compared with 103.5 and 102.6 cm^{-3} in the CTL and SIP experiments (Table 2), respectively. Particularly, SSOA increases the boundary layer CCN concentration

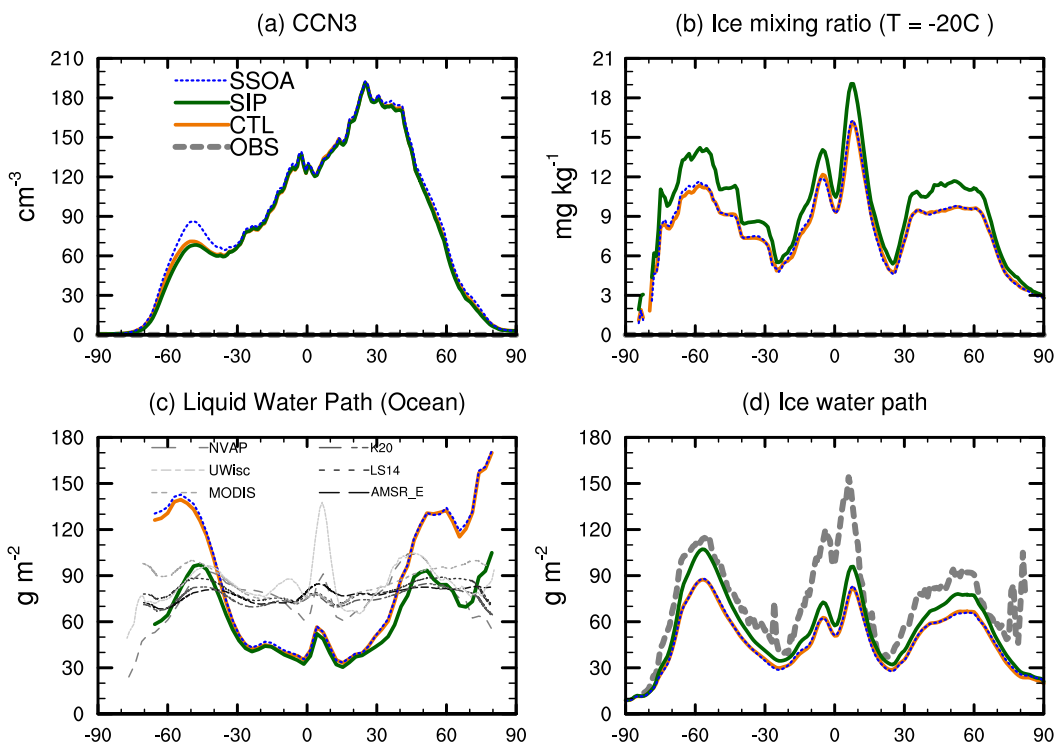

Figure 8. Zonal annual means of (a) surface cloud condensation nuclei (CCN) at 0.1% supersaturation, (b) ice mixing ratio at isotherm of −20°C, (c) liquid water path over the ocean, and (d) ice water path from three model experiments and available observations. Six LWP observational data sets are used in the model evaluation, including the NVAP (NASA Water Vapor Project) LWP data set (Amenu & Kumar, 2005; Randel et al., 1996); the AMSR-E (Advanced Microwave Scanning Radiometer for Earth Observing System) data set (Greenwald et al., 2018); the UWisc (University of Wisconsin) LWP data (O'Dell et al., 2008); and three MODIS (Moderate Resolution Imaging Spectroradiometer) LWP data sets including the original MODIS data (Platnick et al., 2003) and two improved data (Khanal et al., 2020; Lebsock & Su, 2014). IWP observation data are from the CloudSat version 5.1 with an estimated bias of ±40% (Waliser et al., 2009).

Table 2
Annual Means of Marine Boundary Layer CCN Concentrations at 0.1% Supersaturation; Total Grid Box Cloud Liquid Water Path (LWP); Total Grid Box Cloud Ice Water Path (IWP); Shortwave and Longwave Cloud Radiative Effects (SWCRE, LWCRE) at the Top of the Atmosphere; Total Cloud Fraction (CLDTOT); and Total Surface Precipitation Rate (PRECT), Averaged Globally and Over the Southern Hemisphere (SH) (20°–90°S) From the CTL, SIP, and SSOA Simulations

	Global			SH (20°–90°S)		
	CTL	SIP	SSOA	CTL	SIP	SSOA
CCN (cm^{-3})	103.5	102.6	107.0	61.4	57.8	69.1
LWP ($g\ m^{-2}$)	66.9	52.4	67.9	124.3	79.2	128.6
IWP ($g\ m^{-2}$)	50.7	59.3	50.8	74.5	91.3	75.1
LWCRE ($W\ m^{-2}$)	23.8	22.9	23.9	27.4	25.6	27.7
SWCRE ($W\ m^{-2}$)	−47.8	−45.8	−48.2	−71.4	−64.4	−72.4
CLDTOT (%)	68.9	68.5	69.0	92.8	92.1	93.1
PRECT ($mm\ d^{-1}$)	2.88	2.89	2.88	2.91	2.96	2.96

averaged between 40°S and 70°S from 70 cm^{-3} in the CTL experiment to 90 cm^{-3} in the SSOA experiment. As a result, a stronger global mean SWCRE of −48.2 W m^{-2} is found in the SSOA experiment compared with −47.8 W m^{-2} in the CTL experiment (Table 2), while LWCRE is similar between the SSOA and CTL experiments.

Meanwhile, SIP shows a remarkable impact on LWP and IWP. The global mean LWP decreased from 66.9 g m^{-2} in the CTL experiment to 52.4 g m^{-2} in the SIP experiment (detailed discussion on physical processes that cause this decrease in LWP is shown in Zhao and Liu (2021)), most notably in midlatitudes and high latitudes while the global IWP increases from 50.7 g m^{-2} in the CTL experiment to 59.3 g m^{-2} in the SIP experiment (Table 2), suggesting SIP is the dominant ice production process for SO clouds. Global mean SWCRE (LWCRE) is weakened by 2.0 (0.9) W m^{-2} in the SIP experiment compared to the CTL experiment (Table 2). The global annual mean precipitation is similar between these simulations with prescribed sea surface temperatures based on the "Radiative-Convective Equilibrium" (Manabe & Strickler, 1964). Cloud fraction in the model is parameterized based on relative humidity, not directly on condensate amounts. With the same sea surface temperatures, the global mean total cloud fraction is also similar between these simulations (Table 2).

4. Conclusions and Discussion

Based on observational data obtained during the SOCRATES campaign, this paper aims to bridge the gap between recent observational findings and new model developments. An integrated model-observational study is conducted to address the key ice formation processes that control the cloud phase over the pristine remote SO. This work is an extension of our previous model development work which implemented the SSOA and SIP processes in the model, but focused more on the model evaluation against the observational data.

The SSOA influence on the temporal evolution and spatial distribution of CCN concentrations is analyzed. Our results indicate that SSOA increases the CCN number concentrations at 0.1% supersaturation in the marine boundary layer by 50% on average and up to 2 orders of magnitude during the time period of the SOCRATES campaign. A better temporal evolution and vertical distribution of CCN compared to the observations are achieved after considering SSOA in the model.

Furthermore, the importance of SSOA to serve as INPs in the ice nucleation process is also highlighted in this study. The model underestimates the INP concentrations by 1 order of magnitude if only dust is considered. The model eliminates this underestimation if both dust and SSOA are considered in the ice nucleation process, suggesting that the SSOA is the dominant source of INPs over the SO.

To investigate the SIP impact on Ni, a detailed comparison between model and measurement data is conducted. We find that after the model incorporates the two new SIP processes, a better agreement is obtained between the modeled and measured Ni, and the Ni are enhanced by 1–3 orders of magnitude by the SIP processes. Primary ice

nucleation is more important than SIP in cold clouds with temperatures less than −25°C, while the SIP is favored in moderately cold clouds with temperatures greater than −20°C.

This study also conducts statistical analysis to investigate the SIP impact on the cloud phase. Overall, SIP results in more occurrences of mixed-phase and ice-only clouds and fewer occurrences of liquid-only clouds over the SO. The predicted mixed-phase percentage occurrence increases from 15% to 21%, in better agreement with the observations (23%).

The missing processes relevant to the ice formation, in terms of ice nucleation of SSOA and SIP processes, limit our ability to understand the cloud feedback over the SO and climate sensitivity. This study highlights the importance of GCMs to accurately represent the SSOA INPs and SIP and to simulate the cloud phase and cloud feedback over the remote Southern Oceans.

Beyond cloud microphysics, cloud macrophysics in CAM6 and other GCMs remain subject to substantial structural uncertainty, which could confound the representation of cloud microphysics. For example,: (a) Cloud drop number depends strongly on in-cloud vertical velocity, for example, McFiggans et al. (2006). The relevant variations in in-cloud vertical velocity are sub-grid in GCMs, and these sub-grid variations are only parameterized by cloud macrophysics parameterizations (e.g., CLUBB). (b) Cloud fraction (determined by macrophysics parameterizations) has an important control on microphysics. It can significantly mediate the microphysical behavior. Therefore, more efforts at synthesizing the remaining challenges in improving the overall microphysical realism in GCMs are needed.

Data Availability Statement

The model code is available at https://github.com/ESCOMP/CESM. The IWP data (Deng et al., 2015) are available at https://www.cloudsat.cira.colostate.edu/data-products/2c-ice, the data are available for data ordering and download via SFTP with registration. The LWP data (Randel et al., 1996) are available at https://rda.ucar.edu/datasets/ds722.0/, the data are available with registration. The SOCRATES observation data (McFarquhar et al., 2021) are available at https://data.eol.ucar.edu/dataset/552.047. The code used in this study is available at https://doi.org/10.5281/zenodo.7566759. The model output data sets are available at https://doi.org/10.5281/zenodo.7566767.

Acknowledgments
Xiaohong Liu, Xi Zhao, and Yang Shi acknowledge the funding support from the US Department of Energy (DOE) Atmospheric System Research (ASR) Program (Grant DE-SC0020510). Xiaohong Liu and Xi Zhao also acknowledge the funding support from the DOE Regional and Global Model Analysis (RGMA) Program (Grant DE-SC0022065). Susannah Burrows was funded by the U.S. Department of Energy (DOE), Office of Science, Office of Biological and Environmental Research through the Early Career Research Program. Paul J. DeMott acknowledges the National Science Foundation (NSF) Grant AGS-1660486 for data collected from the SOCRATES campaign, and United States Department of Energy Grant DE-SC0021116 for support during manuscript preparation. Vaughan T. J. Phillip was supported by research grants, related to the microphysical properties of cold clouds, from the Swedish Research Council for Sustainable Development (FORMAS; Award 2018-01795), Swedish Research Council (VR; Award 2015-05104), U.S. Department of Energy Atmospheric Sciences Research Program (Award DE-SC0018932), and Sweden's Innovation Agency (Vinnova; 2020-03406). Sachin Patade was supported by the Vinnova Grant. Kevin J. Sanchez and Greg C. Roberts acknowledge the support of NSF Grant AGS-1660374. Minghui Diao acknowledges funding support from DOE ASR Grant DE-SC0021211 and NSF OPP Grant 1744965. Meng Zhang worked under the auspices of the U.S. DOE by Lawrence Livermore National Laboratory under Contract no. DE-AC52-07NA27344. Greg M. McFarquhar was supported by the National Science Foundation (NSF) through Grants AGS-1628674 and AGS-1762096. The measured data were collected using NSF's Lower Atmosphere Observing Facilities, which are managed and operated by the National Center for Atmospheric Research's (NCAR) Earth Observing Laboratory. The authors thank the pilots, mechanics, technicians, scientists, software engineers, and project managers of the NCAR EOL Research Aviation Facility for their support in the field and in post-processing data. The authors would like to thank the Australian Bureau of Meteorology Tasmanian regional Office for the excellent forecast support and weather briefings provided during the field campaign with special thanks to Scott Carpentier, Michelle Hollister, Matthew Thomas, and Robert Schaap.

References

Abdul-Razzak, H., & Ghan, S. J. (2000). A parameterization of aerosol activation: 2. Multiple aerosol types. *Journal of Geophysical Research*, *105*(D5), 6837–6844. https://doi.org/10.1029/1999JD901161

Amenu, G. G., & Kumar, P. (2005). NVAP and reanalysis-2 global precipitable water products: Intercomparison and variability studies. *Bulletin of the American Meteorological Society*, *86*(2), 245–256. https://doi.org/10.1175/BAMS-86-2-245

Atlas, R. L., Bretherton, C. S., Khairoutdinov, M. F., & Blossey, P. N. (2022). Hallett-Mossop rime splintering dims cumulus clouds over the Southern Ocean: New insight from nudged global storm-resolving simulations. *AGU Advances*, *3*(2), e2021AV000454. https://doi.org/10.1029/2021AV000454

Baker, B. A., & Lawson, R. P. (2006). In situ observations of the microphysical properties of wave, cirrus, and anvil clouds. Part I: Wave clouds. *Journal of the Atmospheric Sciences*, *63*(12), 3160–3185. https://doi.org/10.1175/JAS3802.1

Baumgardner, D., & Korolev, A. (1997). Airspeed corrections for optical array probe sample volumes. *Journal of Atmospheric and Oceanic Technology*, *14*(5), 1224–1229. https://doi.org/10.1175/1520-0426(1997)014<1224:ACFOAP>2.0.CO;2

Bodas-Salcedo, A., Hill, P. G., Furtado, K., Williams, K. D., Field, P. R., Manners, J. C., et al. (2016). Large contribution of supercooled liquid clouds to the solar radiation budget of the Southern Ocean. *Journal of Climate*, *29*(11), 4213–4228. https://doi.org/10.1175/JCLI-D-15-0564.1

Bodas-Salcedo, A., Mulcahy, J. P., Andrews, T., Williams, K. D., Ringer, M. A., Field, P. R., & Elsaesser, G. S. (2019). Strong dependence of atmospheric feedbacks on mixed-phase microphysics and aerosol-cloud interactions in HadGEM3. *Journal of Advances in Modeling Earth Systems*, *11*(6), 1735–1758. https://doi.org/10.1029/2019MS001688

Burrows, S. M., Easter, R., Liu, X., Ma, P. L., Wang, H., Elliott, S. M., et al. (2022). OCEANFILMS (Organic Compounds from Ecosystems to Aerosols: Natural Films and Interfaces via Langmuir Molecular Surfactants) sea spray organic aerosol emissions – Implementation in a global climate model and impacts on clouds. *Atmospheric Chemistry and Physics*, *22*(8), 5223–5251. https://doi.org/10.5194/acp-22-5223-2022

Burrows, S. M., Ogunro, O., Frossard, A. A., Russell, L. M., Rasch, P. J., & Elliott, S. M. (2014). A physically based framework for modeling the organic fractionation of sea spray aerosol from bubble film Langmuir equilibria. *Atmospheric Chemistry and Physics*, *14*(24), 13601–13629. https://doi.org/10.5194/acp-14-13601-2014

D'Alessandro, J. J., McFarquhar, G. M., Wu, W., Stith, J. L., Jensen, J. B., & Rauber, R. M. (2021). Characterizing the occurrence and spatial heterogeneity of liquid, ice, and mixed phase low-level clouds over the Southern Ocean using in situ observations acquired during SOCRATES. *Journal of Geophysical Research: Atmospheres*, *126*(11), e2020JD034482. https://doi.org/10.1029/2020JD034482

Danabasoglu, G., Lamarque, J. F., Bacmeister, J., Bailey, D. A., DuVivier, A. K., Edwards, J., et al. (2020). The Community Earth System Model Version 2 (CESM2). *Journal of Advances in Modeling Earth Systems*, *12*(2), e2019MS001916. https://doi.org/10.1029/2019MS001916

DeMott, P. J., Hill, T. C. J., McCluskey, C. S., Prather, K. A., Collins, D. B., Sullivan, R. C., et al. (2016). Sea spray aerosol as a unique source of ice nucleating particles. *Proceedings of the National Academy of Sciences of the United States of America*, *113*(21), 5797–5803. https://doi.org/10.1073/pnas.1514034112

DeMott, P. J., Prenni, A. J., Liu, X., Kreidenweis, S. M., Petters, M. D., Twohy, C. H., et al. (2010). Predicting global atmospheric ice nuclei distributions and their impacts on climate. *Proceedings of the National Academy of Sciences of the United States of America*, *107*(25), 11217–11222. https://doi.org/10.1073/pnas.0910818107

DeMott, P. J., Prenni, A. J., McMeeking, G. R., Sullivan, R. C., Petters, M. D., Tobo, Y., et al. (2015). Integrating laboratory and field data to quantify the immersion freezing ice nucleation activity of mineral dust particles. *Atmospheric Chemistry and Physics*, *15*(1), 393–409. https://doi.org/10.5194/acp-15-393-2015

Deng, M., Mace, G. G., Wang, Z., & Berry, E. (2015). CloudSat 2C-ICE product update with a new Ze parameterization in lidar-only region. [Dataset]. Journal of Geophysical Research: Atmospheres, *120*, 12198–12208. https://doi.org/10.1002/2015JD023600

Field, P. R., Lawson, R. P., Brown, P. R. A., Lloyd, G., Westbrook, C., Moisseev, D., et al. (2017). Chapter 7. Secondary Ice Production – Current state of the science and recommendations for the future. *Meteorological Monographs*, *58*(1), 71–720. https://doi.org/10.1175/AMSMONOGRAPHS-D-16-0014.1

Gantt, B., Meskhidze, N., Facchini, M. C., Rinaldi, M., Ceburnis, D., & O'Dowd, C. D. (2011). Wind speed dependent size-resolved parameterization for the organic mass fraction of sea spray aerosol. *Atmospheric Chemistry and Physics*, *11*(16), 8777–8790. https://doi.org/10.5194/acp-11-8777-2011

Gettelman, A., Hannay, C., Bacmeister, J. T., Neale, R. B., Pendergrass, A. G., Danabasoglu, G., et al. (2019). High climate sensitivity in the Community Earth System Model Version 2 (CESM2). *Geophysical Research Letters*, *46*(14), 8329–8337. https://doi.org/10.1029/2019GL083978

Gettelman, A., & Morrison, H. (2015). Advanced two-moment bulk microphysics for global models. Part I: Off-line tests and comparison with other schemes. *Journal of Climate*, *28*(3), 1268–1287. https://doi.org/10.1175/JCLI-D-14-00102.1

Golaz, J. C., Larson, V. E., & Cotton, W. R. (2002). A PDF-based model for boundary layer clouds. Part I: Method and model description. *Journal of the Atmospheric Sciences*, *59*(24), 3540–3551. https://doi.org/10.1175/1520-0469(2002)059<3540:APBMFB>2.0.CO;2

Greenwald, T. J., Bennartz, R., Lebsock, M., & Teixeira, J. (2018). An uncertainty data set for passive microwave satellite observations of warm cloud liquid water path. *Journal of Geophysical Research: Atmospheres*, *123*(7), 3668–3687. https://doi.org/10.1002/2017JD027638

Hallett, J., & Mossop, S. C. (1974). Production of secondary ice particles during the riming process. *Nature*, *249*(5452), 26–28. https://doi.org/10.1038/249026a0

Hoose, C., Kristjánsson, J. E., Chen, J. P., & Hazra, A. (2010). A classical-theory-based parameterization of heterogeneous ice nucleation by mineral dust, soot, and biological particles in a global climate model. *Journal of the Atmospheric Sciences*, *67*(8), 2483–2503. https://doi.org/10.1175/2010JAS3425.1

Huang, W. T. K., Ickes, L., Tegen, I., Rinaldi, M., Ceburnis, D., & Lohmann, U. (2018). Global relevance of marine organic aerosol as ice nucleating particles. *Atmospheric Chemistry and Physics*, *18*(15), 11423–11445. https://doi.org/10.5194/acp-18-11423-2018

Huang, Y., Blyth, A. M., Brown, P. R. A., Choularton, T. W., & Cui, Z. (2017). Factors controlling secondary ice production in cumulus clouds. *Quarterly Journal of the Royal Meteorological Society*, *143*(703), 1021–1031. https://doi.org/10.1002/qj.2987

Järvinen, E., McCluskey, C. S., Waitz, F., Schnaiter, M., Bansemer, A., Bardeen, C. G., et al. (2022). Evidence for secondary ice production in southern ocean maritime boundary layer clouds. *Journal of Geophysical Research: Atmospheres*, *127*(16), e2021JD036411. https://doi.org/10.1029/2021JD036411

Kay, J. E., Hillman, B. R., Klein, S. A., Zhang, Y., Medeiros, B., Pincus, R., et al. (2012). Exposing global cloud biases in the community atmosphere model (CAM) using satellite observations and their corresponding instrument simulators. *Journal of Climate*, *25*(15), 5190–5207. https://doi.org/10.1175/JCLI-D-11-00469.1

Ke, Z., Liu, X., Wu, M., Shan, Y., & Shi, Y. (2022). Improved dust representation and impacts on dust transport and radiative effect in CAM5. *Journal of Advances in Modeling Earth Systems*, *14*(7), e2021MS002845. https://doi.org/10.1029/2021MS002845

Khanal, S., Wang, Z., & French, J. R. (2020). Improving middle and high latitude cloud liquid water path measurements from MODIS. *Atmospheric Research*, *243*, 105033. https://doi.org/10.1016/j.atmosres.2020.105033

Larson, V. E., Golaz, J.-C., & Cotton, W. R. (2002). Small-scale and mesoscale variability in cloudy boundary layers: Joint probability density functions. *Journal of the Atmospheric Sciences*, *59*(24), 3519–3539. https://doi.org/10.1175/1520-0469(2002)059<3519:SSAMVI>2.0.CO;2

Lasher-Trapp, S., Scott, E. L., Järvinen, E., Schnaiter, M., Waitz, F., DeMott, P. J., et al. (2021). Observations and modeling of rime splintering in Southern Ocean cumuli. *Journal of Geophysical Research: Atmospheres*, *126*(23), e2021JD035479. https://doi.org/10.1029/2021JD035479

Lebsock, M., & Su, H. (2014). Application of active spaceborne remote sensing for understanding biases between passive cloud water path retrievals. *Journal of Geophysical Research: Atmospheres*, *119*(14), 8962–8979. https://doi.org/10.1002/2014JD021568

Li, L., Mahowald, N. M., Kok, J. F., Liu, X., Wu, M., Leung, D. M., et al. (2022). Importance of different parameterization changes for the updated dust cycle modeling in the Community Atmosphere Model (version 6.1). *Geoscientific Model Development*, *15*(22), 8181–8219. https://doi.org/10.5194/gmd-15-8181-2022

Liu, X., Easter, R. C., Ghan, S. J., Zaveri, R., Rasch, P., Shi, X., et al. (2012). Toward a minimal representation of aerosols in climate models: Description and evaluation in the Community Atmosphere Model CAM5. *Geoscientific Model Development*, *5*(3), 709–739. https://doi.org/10.5194/gmd-5-709-2012

Liu, X., Ma, P. L., Wang, H., Tilmes, S., Singh, B., Easter, R. C., et al. (2016). Description and evaluation of a new four-mode version of the Modal Aerosol Module (MAM4) within version 5.3 of the Community Atmosphere Model. *Geoscientific Model Development*, *9*(2), 505–522. https://doi.org/10.5194/gmd-9-505-2016

Liu, X., & Penner, J. E. (2005). Ice nucleation parameterization for global models. *Meteorologische Zeitschrift*, *14*(4), 499–514. https://doi.org/10.1127/0941-2948/2005/0059

Liu, X., Xie, S., & Ghan, S. J. (2007). Evaluation of a new mixed-phase cloud microphysics parameterization with CAM3 single-column model and M-PACE observations. *Geophysical Research Letters*, *34*(23), L23712. https://doi.org/10.1029/2007GL031446

Mace, G. G., Benson, S., & Hu, Y. (2020). On the frequency of occurrence of the ice phase in supercooled Southern Ocean low clouds derived from CALIPSO and CloudSat. *Geophysical Research Letters*, *47*(14), e2020GL087554. https://doi.org/10.1029/2020GL087554

Mace, G. G., Zhang, Q., Vaughan, M., Marchand, R., Stephens, G., Trepte, C., & Winker, D. (2009). A description of hydrometeor layer occurrence statistics derived from the first year of merged Cloudsat and CALIPSO data. *Journal of Geophysical Research*, *114*, D00A26. https://doi.org/10.1029/2007JD009755

Manabe, S., & Strickler, R. F. (1964). Thermal equilibrium of the atmosphere with a convective adjustment. *Journal of the Atmospheric Sciences*, *21*(4), 361–385. https://doi.org/10.1175/1520-0469(1964)021<0361:TEOTAW>2.0.CO;2

Matus, A. V., & L'Ecuyer, T. S. (2017). The role of cloud phase in Earth's radiation budget. *Journal of Geophysical Research: Atmospheres*, *122*(5), 2559–2578. https://doi.org/10.1002/2016JD025951

McCluskey, C. S., DeMott, P. J., Ma, P. L., & Burrows, S. M. (2019). Numerical representations of marine ice-nucleating particles in remote marine environments evaluated against observations. *Geophysical Research Letters*, *46*(13), 7838–7847. https://doi.org/10.1029/2018gl081861

McCluskey, C. S., Hill, T. C. J., Humphries, R. S., Rauker, A. M., Moreau, S., Strutton, P. G., et al. (2018). Observations of ice nucleating particles over Southern Ocean waters. *Geophysical Research Letters*, *45*(21), 11989–11997. https://doi.org/10.1029/2018GL079981

McCluskey, C. S., Ovadnevaite, J., Rinaldi, M., Atkinson, J., Belosi, F., Ceburnis, D., et al. (2018). Marine and terrestrial organic ice-nucleating particles in pristine marine to continentally influenced Northeast Atlantic air masses. *Journal of Geophysical Research: Atmospheres*, *123*(11), 6196–6212. https://doi.org/10.1029/2017JD028033

McCoy, D. T., Hartmann, D. L., & Grosvenor, D. P. (2014). Observed Southern Ocean cloud properties and shortwave reflection. Part II: Phase changes and low cloud feedback. *Journal of Climate*, *27*(23), 8858–8868. https://doi.org/10.1175/JCLI-D-14-00288.1

McFarquhar, G. M., Bretherton, C. S., Marchand, R., Protat, A., DeMott, P. J., Alexander, S. P., et al. (2021). Observations of clouds, aerosols, precipitation, and surface radiation over the Southern Ocean: An overview of CAPRICORN, MARCUS, MICRE, and SOCRATES. [Dataset]. Bulletin of the American Meteorological Society, *102*(4), E894–E928. https://doi.org/10.1175/BAMS-D-20-0132.1

McFarquhar, G. M., Finlon, J. A., Stechman, D. M., Wu, W., Jackson, R., & Freer, M., (2018). University of Illinois/Oklahoma Optical Array Probe (OAP) Processing Software, 2018, Software, Zenodo. https://doi.org/10.5281/zenodo.1285968

McFiggans, G., Artaxo, P., Baltensperger, U., Coe, H., Facchini, M. C., Feingold, G., et al. (2006). The effect of physical and chemical aerosol properties on warm cloud droplet activation. *Atmospheric Chemistry and Physics*, *6*(9), 2593–2649. https://doi.org/10.5194/acp-6-2593-2006

Meskhidze, N., Xu, J., Gantt, B., Zhang, Y., Nenes, A., Ghan, S. J., et al. (2011). Global distribution and climate forcing of marine organic aerosol: 1. Model improvements and evaluation. *Atmospheric Chemistry and Physics*, *11*(22), 11689–11705. https://doi.org/10.5194/acp-11-11689-2011

Meyers, M. P., Demott, P. J., & Cotton, W. R. (1992). New primary ice-nucleation parameterizations in an explicit cloud model. *Journal of Applied Meteorology*, *31*(7), 708–721. https://doi.org/10.1175/1520-0450(1992)031<0708:NPINPI>2.0.CO;2

Molod, A., Takacs, L., Suarez, M., & Bacmeister, J. (2015). Development of the GEOS-5 atmospheric general circulation model: Evolution from MERRA to MERRA2. *Geoscientific Model Development*, *8*(5), 1339–1356. https://doi.org/10.5194/GMD-8-1339-2015

Morrison, H., De Boer, G., Feingold, G., Harrington, J., Shupe, M. D., & Sulia, K. (2012). Resilience of persistent Arctic mixed-phase clouds. *Nature Geoscience*, *5*, 11–17.

Murray, B. J., Carslaw, K. S., & Field, P. R. (2021). Opinion: Cloud-phase climate feedback and the importance of ice-nucleating particles. *Atmospheric Chemistry and Physics*, *21*(2), 665–679. https://doi.org/10.5194/ACP-21-665-2021

Niemand, M., Mohler, O., Vogel, B., Vogel, H., Hoose, C., Connolly, P., et al. (2012). A particle-surface-area-based parameterization of immersion freezing on desert dust particles. *Journal of the Atmospheric Sciences*, *69*(10), 3077–3092. https://doi.org/10.1175/JAS-D-11-0249.1

O'Dell, C. W., Wentz, F. J., & Bennartz, R. (2008). Cloud liquid water path from satellite-based passive microwave observations: A new climatology over the global oceans. *Journal of Climate*, *21*(8), 1721–1739. https://doi.org/10.1175/2007JCLI1958.1

O'Shea, J. S., Choularton, T. W., Flynn, M., Bower, K. N., Gallagher, M., Crosier, J., et al. (2017). In situ measurements of cloud microphysics and aerosol over coastal Antarctica during the MAC campaign. *Atmospheric Chemistry and Physics*, *17*(21), 13049–13070. https://doi.org/10.5194/ACP-17-13049-2017

O'Shea, S., Crosier, J., Dorsey, J., Gallagher, L., Schledewitz, W., Bower, K., et al. (2021). Characterising optical array particle imaging probes: Implications for small-ice-crystal observations. *Atmospheric Measurement Techniques*, *14*(3), 1917–1939. https://doi.org/10.5194/amt-14-1917-2021

Phillips, V. T. J., Patade, S., Gutierrez, J., & Bansemer, A. (2018). Secondary ice production by fragmentation of freezing drops: Formulation and theory. *Journal of the Atmospheric Sciences*, *75*(9), 3031–3070. https://doi.org/10.1175/JAS-D-17-0190.1

Phillips, V. T. J., Yano, J. I., Formenton, M., Ilotoviz, E., Kanawade, V., Kudzotsa, I., et al. (2017). Ice multiplication by breakup in ice-ice collisions. Part II: Numerical simulations. *Journal of the Atmospheric Sciences*, *74*(9), 2789–2811. https://doi.org/10.1175/jas-d-16-0223.1

Phillips, V. T. J., Yano, J. I., & Khain, A. (2017). Ice multiplication by breakup in ice-ice collisions. Part I: Theoretical formulation. *Journal of the Atmospheric Sciences*, *74*(6), 1705–1719. https://doi.org/10.1175/JAS-D-16-0224.1

Platnick, S., King, M. D., Ackerman, S. A., Menzel, W. P., Baum, B. A., Riédi, J. C., & Frey, R. A. (2003). The MODIS cloud products: Algorithms and examples from terra. *IEEE Transactions on Geoscience and Remote Sensing*, *41*(2), 459–472. https://doi.org/10.1109/TGRS.2002.808301

Randel, D. L., Vonder Haar, T. H., Ringerud, M. A., Stephens, G. L., Greenwald, T. J., & Combs, C. L. (1996). A new global water vapor dataset. [Dataset]. Bulletin of the American Meteorological Society, *77*(6), 1233–1246. https://doi.org/10.1175/1520-0477(1996)077<1233:ANGWVD>2.0.CO;2

Roberts, G. C., & Nenes, A. (2005). A continuous-flow streamwise thermal-gradient CCN chamber for atmospheric measurements. *Aerosol Science and Technology*, *39*(3), 206–221. https://doi.org/10.1080/027868290913988

Sanchez, K. J., Roberts, G. C., Saliba, G., Russell, L. M., Twohy, C., Reeves, M. J., et al. (2021). Measurement report: Cloud processes and the transport of biological emissions affect southern ocean particle and cloud condensation nuclei concentrations. *Atmospheric Chemistry and Physics*, *21*(5), 3427–3446. https://doi.org/10.5194/ACP-21-3427-2021

Tan, I., Oreopoulos, L., & Cho, N. (2019). The role of thermodynamic phase shifts in cloud optical depth variations with temperature. *Geophysical Research Letters*, *46*(8), 4502–4511. https://doi.org/10.1029/2018GL081590

Tan, I., Storelvmo, T., & Zelinka, M. D. (2016). Observational constraints on mixed-phase clouds imply higher climate sensitivity. *Science*, *352*(6282), 224–227. https://doi.org/10.1126/science.aad5300

Terai, C. R., Zelinka, M., & Klein, S. A. (2016). Constraining the low-cloud optical depth feedback at middle and high latitudes using satellite observations. *Journal of Geophysical Research: Atmospheres*, *121*(16), 9696–9716. https://doi.org/10.1002/2016JD025233

Vergara-Temprado, J., Holden, M. A., Orton, T. R., O'Sullivan, D., Umo, N. S., Browse, J., et al. (2018). Is black carbon an unimportant ice-nucleating particle in mixed-phase clouds? *Journal of Geophysical Research: Atmospheres*, *123*(8), 4273–4283. https://doi.org/10.1002/2017JD027831

Waliser, D. E., Li, J. L. F., Woods, C. P., Austin, R. T., Bacmeister, J., Chern, J., et al. (2009). Cloud ice: A climate model challenge with signs and expectations of progress. *Journal of Geophysical Research*, *114*, D00A21. https://doi.org/10.1029/2008jd010015

Wang, Y., Liu, X., Hoose, C., & Wang, B. (2014). Different contact angle distributions for heterogeneous ice nucleation in the Community Atmospheric Model version 5. *Atmospheric Chemistry and Physics*, *14*(19), 10411–10430. https://doi.org/10.5194/acp-14-10411-2014

Wang, Y., McFarquhar, G. M., Rauber, R. M., Zhao, C., Wu, W., Finlon, J. A., et al. (2020). Microphysical properties of generating cells over the Southern Ocean: Results from SOCRATES. *Journal of Geophysical Research: Atmospheres*, *125*(13), e2019JD032237. https://doi.org/10.1029/2019JD032237

Wang, Y., Zhang, D., Liu, X., & Wang, Z. (2018). Distinct contributions of ice nucleation, large-scale environment, and shallow cumulus detrainment to cloud phase partitioning with NCAR CAM5. *Journal of Geophysical Research: Atmospheres*, *123*(2), 1132–1154. https://doi.org/10.1002/2017JD027213

Wilson, T. W., Ladino, L. A., Alpert, P. A., Breckels, M. N., Brooks, I. M., Browse, J., et al. (2015). A marine biogenic source of atmospheric ice-nucleating particles. *Nature*, *525*(7568), 234–238. https://doi.org/10.1038/nature14986

Wu, C., Liu, X., Diao, M., Zhang, K., Gettelman, A., Lu, Z., et al. (2017). Direct comparisons of ice cloud macro- and microphysical properties simulated by the Community Atmosphere Model version 5 with HIPPO aircraft observations. *Atmospheric Chemistry and Physics*, *17*(7), 4731–4749. https://doi.org/10.5194/acp-17-4731-2017

Wu, M., Liu, X., Yu, H., Wang, H., Shi, Y., Yang, K., et al. (2020). Understanding processes that control dust spatial distributions with global climate models and satellite observations. *Atmospheric Chemistry and Physics*, *20*(22), 13835–13855. https://doi.org/10.5194/acp-20-13835-2020

Yang, C. A., Diao, M., Gettelman, A., Zhang, K., Sun, J., McFarquhar, G., & Wu, W. (2021). Ice and supercooled liquid water distributions over the Southern Ocean based on in situ observations and climate model simulations. *Journal of Geophysical Research: Atmospheres*, *126*(24), e2021JD036045. https://doi.org/10.1029/2021JD036045

Zaremba, T. J., Rauber, R. M., McFarquhar, G. M., Hayman, M., Finlon, J. A., & Stechman, D. M. (2020). Phase characterization of cold sector Southern Ocean cloud tops: Results from SOCRATES. *Journal of Geophysical Research: Atmospheres*, *125*(24), e2020JD033673. https://doi.org/10.1029/2020JD033673

Zelinka, M. D., Myers, T. A., McCoy, D. T., Po-Chedley, S., Caldwell, P. M., Ceppi, P., et al. (2020). Causes of higher climate sensitivity in CMIP6 models. *Geophysical Research Letters*, *47*(1), e2019GL085782. https://doi.org/10.1029/2019GL085782

Zhang, M., Liu, X., Diao, M., D'Alessandro, J. J., Wang, Y., Wu, C., et al. (2019). Impacts of representing heterogeneous distribution of cloud liquid and ice on phase partitioning of Arctic mixed-phase clouds with NCAR CAM5. *Journal of Geophysical Research: Atmospheres*, *124*(23), 13071–13090. https://doi.org/10.1029/2019JD030502

Zhang, G. J., & McFarlane, N. A. (1995). Sensitivity of climate simulations to the parameterization of cumulus convection in the Canadian climate center general circulation model. *Atmosphere-Ocean*, *33*(3), 407–446. https://doi.org/10.1080/07055900.1995.9649539

Zhao, X., & Liu, X. (2021). Global importance of secondary ice production. *Geophysical Research Letters*, *48*(11), e2021GL092581. https://doi.org/10.1029/2021GL092581

Zhao, X., & Liu, X. (2022). Primary and secondary ice production: Interactions and their relative importance. *Atmospheric Chemistry and Physics*, *22*(4), 2585–2600. https://doi.org/10.5194/ACP-22-2585-2022

Zhao, X., Liu, X., Burrows, S. M., & Shi, Y. (2021). Effects of marine organic aerosols as sources of immersion-mode ice-nucleating particles on high-latitude mixed-phase clouds. *Atmospheric Chemistry and Physics*, *21*(4), 2305–2327. https://doi.org/10.5194/acp-21-2305-2021

Zhao, X., Liu, X., Phillips, V. T. J., & Patade, S. (2021). Impacts of secondary ice production on Arctic mixed-phase clouds based on ARM observations and CAM6 single-column model simulations. *Atmospheric Chemistry and Physics*, *21*(7), 5685–5703. https://doi.org/10.5194/acp-21-5685-2021